MABS
2025, VOL. 17, NO. 1, 2502673
https://doi.org/10.1080/19420862.2025.2502673

Taylor & Francis
Taylor & Francis Group

REPORT

OPEN ACCESS Check for updates

Hybrid IgE-IgG1 antibodies (IgEG): a new antibody class that combines IgE and IgG functionality

Melanie Grandits[a,b*], Lais C. G. F. Palhares[a,b*], Olivia Macleod[b], John Devlin[b], Oliver E. Amin[b], James Birtley[b], Leanne Partington[b], Tim Wilson[b], Elizabeth Hardaker[b], Sophia N. Karagiannis[a,b,c], Heather J. Bax[a,b], and Kevin FitzGerald[b]

[a]St. John's Institute of Dermatology, School of Basic & Medical Biosciences, King's College London, London, UK; [b]Epsilogen Ltd, Waterfront, ARC West London, London, UK; [c]Breast Cancer Now Research Unit, School of Cancer & Pharmaceutical Sciences, King's College London, Guy's Hospital, London, UK

ABSTRACT

IgG-based anti-cancer therapies have achieved promising clinical outcomes, but, especially for patients with solid tumors, response rates vary. IgE antibodies promote distinct immune responses compared to IgG and have shown anti-tumoral pre-clinical activity and preliminary efficacy and safety profile in clinical testing. To improve potency further, we engineered a hybrid IgE-IgG1 antibody (IgEG), to combine the functions of both isotypes. Two IgEGs were generated with variable regions taken from trastuzumab (Tras IgEG) and from a novel anti-HER2 IgE (26 IgEG). Both IgEGs expressed well in mammalian cells and demonstrated IgE-like stability. IgEGs demonstrated both IgE and IgG1 functionality *in vitro*. A lack of type I hypersensitivity associated with IgEG incubation with human blood is suggestive of acceptable safety. *In vivo*, IgEGs exhibited distinct pharmacokinetic profiles and produced anti-tumoral efficacy comparable to IgE. These findings highlight the potential of IgEG as a new therapeutic modality in oncology.

ARTICLE HISTORY
Received 6 January 2025
Revised 1 May 2025
Accepted 2 May 2025

KEYWORDS
IgE; IgG; Hybrid; HER2; anti-cancer therapy

Introduction

Monoclonal antibodies (mAbs) have revolutionized treatment for cancer, with significantly improved outcomes achieved in some malignancies. Almost all currently approved mAbs are IgGs, with the majority being of the IgG1 subtype.[1] Beneficial attributes of IgG1 antibodies include long serum half-life (around 23 days) and the ability to activate the immune system *via* a plurality of effector functions, i.e., antibody-dependent cell-mediated cytotoxicity (ADCC) or phagocytosis (ADCP) and complement-dependent cytotoxicity (CDC).[2,3] While IgG1-based therapies can provide improved outcomes for some patients, treatment responses are highly variable.[4] Anti-tumoral responses elicited by IgG1 may be hampered by the immunosuppressive tumor microenvironment (TME), where immune cells may have impaired effector functions and expression of inhibitory FcγRIIb.[5,6] Furthermore, affinity-reducing polymorphisms of FcγRII/IIIA in patients are generally linked to lower responses and poor treatment outcomes.[7,8] Fc engineering to enhance FcγR-binding of therapeutic IgG1s has been utilized with the aim to improve the overall treatment responses. However, the overall survival benefits provided by Fc-modified IgG1 when compared to unmodified therapies have been negligible.[9–11] Therefore, there remains a substantial unmet clinical need for enhanced cancer therapeutics.

Considering these limitations and the complexity of the immune landscape within the TME, optimal responses may additionally require activation of a different arm of the immune system. IgE antibodies bear unique features to those of IgG. These include a lack of inhibitory Fc receptors and a high affinity for cognate FcεR on certain immune effector cells such as mast cells and alternatively activated macrophages which occupy the TME.[12–15] IgE engagement with FcεR-expressing cells can promote potent anti-tumor functions and immune surveillance.[15–19] Together, these properties may be beneficial if directed against antigens on solid tumors. We have previously reported that IgE-based anti-cancer therapies show significant Fc-mediated anti-tumor functions *in vitro* and reduce tumor burden in preclinical models of melanoma, breast and ovarian cancer.[16,18–22] The first-in-class Phase 1 clinical trial of the IgE antibody, MOv18 IgE, has demonstrated good tolerability and signs of efficacy in patients with ovarian cancer.[23] This success has led to the progression of MOv18 IgE to a Phase 1b clinical trial (NCT06547840), as well as substantial investment in developing IgE as a modality for the treatment for various other cancers.

Reasoning that mobilizing both IgG1 and IgE driven immune responses against a single epitope on a tumor-associated antigen might further improve anti-tumor responses, we engineered an antibody that combines IgE-IgG1 functionality (IgEG). In this study, we incorporated the variable domains (Fv) of the anti-HER2 mAb trastuzumab into the IgEG scaffold and evaluated its anti-tumor potential

CONTACT Kevin FitzGerald kevin@epsilogen.com Epsilogen Ltd, Waterfront, ARC West London, Manbre Road, Hammersmith, London W6 9RH, UK
*Equal contribution.
Supplemental data for this article can be accessed online at https://doi.org/10.1080/19420862.2025.2502673.

using trastuzumab IgG1 and trastuzumab IgE as controls. We assessed the expression and stability of trastuzumab IgEG (Tras IgEG) and characterized its biophysical properties and functional profile *in vitro*. We further evaluated the pharmacokinetic properties of IgEGs and their *in vivo* efficacy in a medium/low (Herceptest 2+) hHER2-expressing human breast cancer xenograft model. We investigated whether IgEGs trigger type I hypersensitivity reactions *ex vivo* to provide a first indication of safety. We determined whether IgEGs retain their *in vitro* and *in vivo* properties when their variable domains are taken from an alternative anti-HER2 antibody (clone 26). Finally, we assessed the anti-tumor efficacy of 26 IgEG compared to its IgE and IgG counterparts in an *in vivo* dose–response study.

Overall, this study builds on our prior findings for IgE-based therapeutics to explore the therapeutic potential of a novel therapeutic antibody class that combines IgE and IgG1 functions.

Results

Novel IgEG antibody can be produced at high quality and shows good stability

We engineered a novel IgE-IgG1 hybrid antibody (IgEG), consisting of a full-length IgE connected to an IgG1 Fc-region through an IgG1 hinge (Figure 1a). As the first cysteine of the IgG1 hinge (C220), which usually pairs with a cysteine in the light chain,[24,25] remained free, we substituted it with a serine to avoid potential aggregation or misfolding.

As proof-of-principle of this new antibody class we engineered and produced an IgEG with variable regions taken from the well-characterized anti-HER2 mAb trastuzumab (Tras) (Figure 1a). Tras IgG1 was commercially sourced and Tras IgE was produced as described. Sodium dodecyl sulfate-polyacrylamide electrophoresis (SDS-PAGE) under non-reduced conditions shows fully assembled Tras IgG1, IgE and IgEG at the predicted sizes of around 150, 190 and 255 kDa, respectively (Figure 1b, lanes 1–3), with no degradation products. Under reduced conditions, the heavy chain for IgG1, IgE and IgEG is observed at around 55, 75 and 105 kDa, respectively, with the light chain for all three antibody constructs at around 25 kDa (Figure 1b, lanes 4–6). All three constructs exhibited a high monomer content (>98%) and absence of aggregates or degradation products (size-exclusion chromatography, SEC-HPLC, Figure 1c). Differential scanning fluorimetry (DSF) revealed a similar melting temperature profile for Tras IgEG compared to Tras IgE, but different to that of Tras IgG1 (Figure 1d). Tras IgEG stored for 6 weeks at 4°C, followed by one freeze-thaw cycle at −20°C or −80°C, showed no signs of aggregation or degradation by SEC-HPLC (Figure 1e). Affinity of the differently stored aliquots to human HER2 (hHER2) by surface plasmon resonance (SPR) was unaffected (Figure 1f, Supplementary Figure 1B). These findings confirm the generation of an intact IgEG antibody construct, at high purity and with a good stability profile.

Trastuzumab IgEG displays dual IgE and IgG1 isotype characteristics and functionality in vitro

Biochemical characterization by SPR showed that the affinity of Tras IgEG to hHER2 is comparable to that of Tras IgG1 and Tras IgE (Figure 2a, Supplementary Figure S2A). Affinities of Tras IgEG to FcγRI and FcεRI were also equivalent to Tras IgG1 and IgE, respectively (Figures 2b,c, Supplementary Figure S2B). As expected, no binding of Tras IgG1 to FcεRI, or Tras IgE to FcγRI, was observed (Figures 2b,c). Tras IgEG retained the ability of IgG1 to bind to C1q (Supplementary Figures S2C, 2D). Cell surface binding of the Tras constructs to hHER2-expressing SKBR3 cells, hFcγR-expressing primary natural killer (NK) cells and hFcεRI-expressing RBL-SX38 cells concurred with the SPR results (Figure 2d, Supplementary Figure S2E).

In line with these observations, Tras IgEG triggered FcεRI-mediated degranulation of RBL-SX38 cells, upon crosslinking with SKBR3 cells to a similar level as Tras IgE (Figure 2e). Furthermore, levels of primary NK cell-mediated ADCC (Figure 2f), and healthy volunteer peripheral blood mononuclear cells (PBMC)-mediated total killing (Figure 2g) of SKBR3 cells, was comparable between Tras IgEG and Tras IgG1.

Together these data demonstrate the intended dual-isotype functional attributes of Tras IgEG.

Trastuzumab IgEG shows a distinct pharmacokinetic profile and potent anti-tumoral activity in vivo

IgE antibodies have been shown to have a short serum half-life (2–3 days) in humans. Lack of binding of IgE to the neonatal Fc receptor (FcRn) is one of the reasons for this fast clearance from the circulation.[26] Having confirmed that Tras IgEG possesses both IgE and IgG functionality through binding Fcε and Fcγ receptors, we reasoned that the molecule may also bind to FcRn in a pH-dependent manner, thereby influencing its serum half-life (Suplementary Figure S3A).

SPR analyses confirmed the affinity of Tras IgEG to hFcRn at pH 6.0 was equivalent to Tras IgG1. As expected, Tras IgE lacked hFcRn binding at pH 6.0 and no binding was observed for any of the three isotypes to hFcRn at pH 7.4 (Figure 3a, Supplementary Figure S3B). To determine the pharmacokinetic profile of Tras IgEG in comparison to its IgG1 and IgE counterparts, an FcRn humanized (hFcRn+/mFcRn- Tg32 SCID) mouse model was used. First, an initial assessment using a typical IgG1 blood sampling schedule was performed (Supplementary Figure S3C). Subsequently, sampling schedules were optimized and carried out to best evaluate the pharmacokinetic profile of individual constructs (Figure 3b, Supplementary Figure S3D). In contrast to Tras IgG1 and Tras IgEG, the terminal half-life of Tras IgE could not be determined due to fast clearance, therefore Tras IgE half-life was manually calculated using all data points. Tras IgEG showed a significantly elongated serum half-life compared with Tras IgE, albeit with a shorter half-life compared to Tras IgG1 (Figure 3c).

To assess the Fc-mediated anti-tumoral activity of IgEGs *in vivo*, we utilized a JIMT-1 human breast cancer xenograft

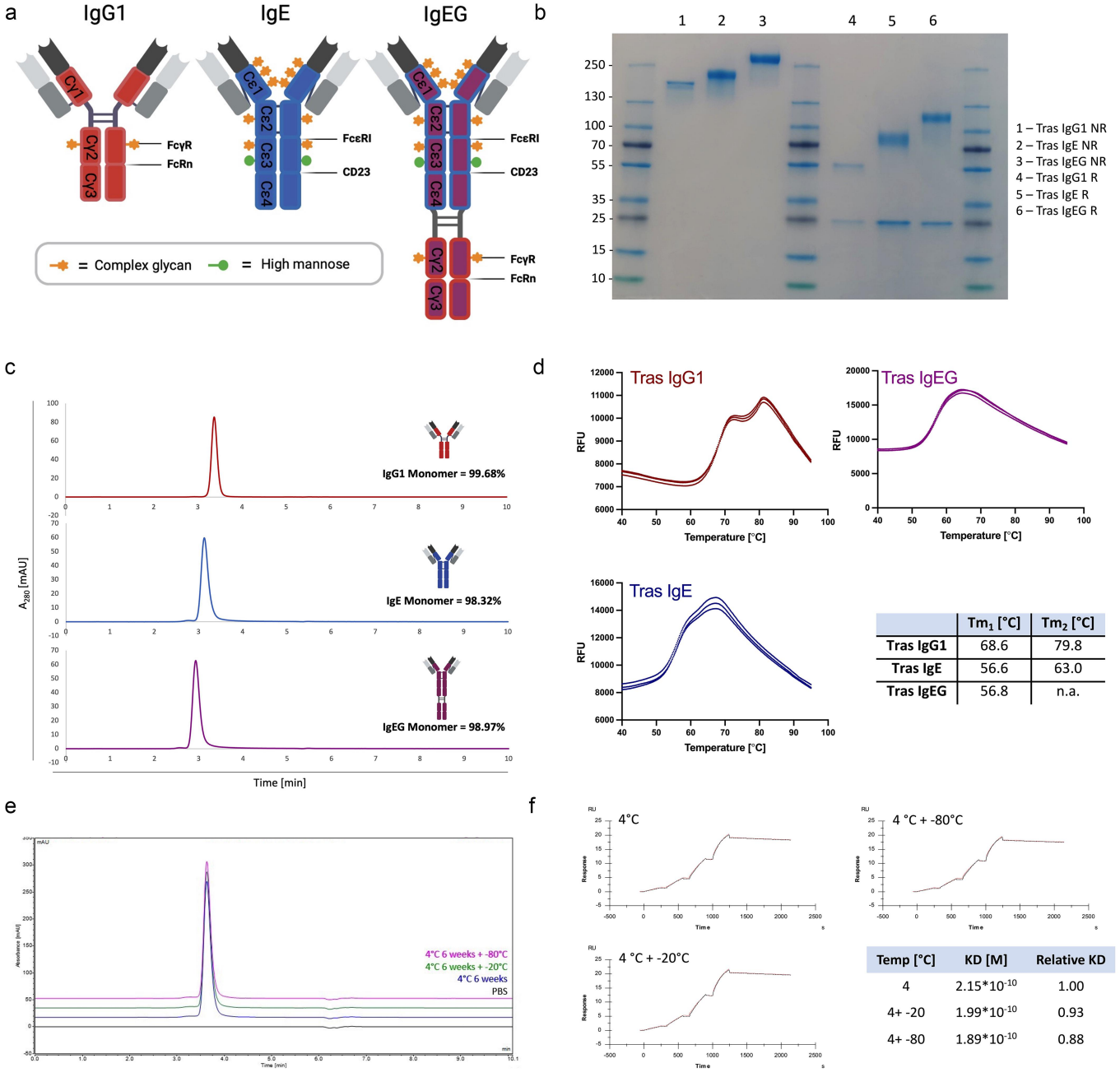

	Tm_1 [°C]	Tm_2 [°C]
Tras IgG1	68.6	79.8
Tras IgE	56.6	63.0
Tras IgEG	56.8	n.a.

Temp [°C]	KD [M]	Relative KD
4	$2.15*10^{-10}$	1.00
4+ -20	$1.99*10^{-10}$	0.93
4+ -80	$1.89*10^{-10}$	0.88

Figure 1. Design, purity and stability of an IgEG antibody construct. (a) schematic of IgG1 (red), IgE (blue) and IgEG (purple) structure. IgEG consists of the variable heavy (dark gray) and the light chains (dark and medium gray) and the complete constant regions of IgE (purple with blue outline), connected to an IgG1 fc-region (purple with red outline) through an IgG1 hinge region. (b) SDS-PAGE of non-reduced (lanes: 1–3) and reduced (lanes: 4–6) Tras IgG1, IgE and IgEG. (c) analytical SEC-HPLC traces showing high purity and monomer content of Tras IgG1, IgE and IgEG. (d) differential scanning fluorimetry showing similar melting profiles and temperatures of Tras IgEG and Tras IgE, which are different to that of Tras IgG1 (n.A.= not applicable). (e) SEC-HPLC chromatograms of Tras IgEG stored for 6 weeks at 4 °C (blue), followed by one freeze-thaw cycle at – 20 °C (green) or – 80 °C (pink), showing intact constructs and absence of aggregation or degradation. (f) surface plasmon resonance (SPR) analysis shows comparable affinity to hHER2 by IgEG following storage under the three conditions above (sensorgrams and KD (M) are shown).

model. JIMT-1 cells are known to be resistant to the Fab-mediated effects of trastuzumab,[27] and feature medium/low HER2 (Herceptest 2+) expression levels. We first confirmed cell-surface binding of Tras IgEG, IgG1 and IgE to JIMT-1 cells *in vitro* (Figure 3d) and IgEG and IgE-mediated RBL-SX38 degranulation upon crosslinking with JIMT-1 cells (Figure 3e). Both IgEG and IgG1 mediated JIMT-1 ADCC by human primary NK cells (Figure 3f). Immunodeficient mice challenged with JIMT-1 tumors were engrafted with human PBMCs and injected biweekly with 120 nmol/kg Tras IgG1,

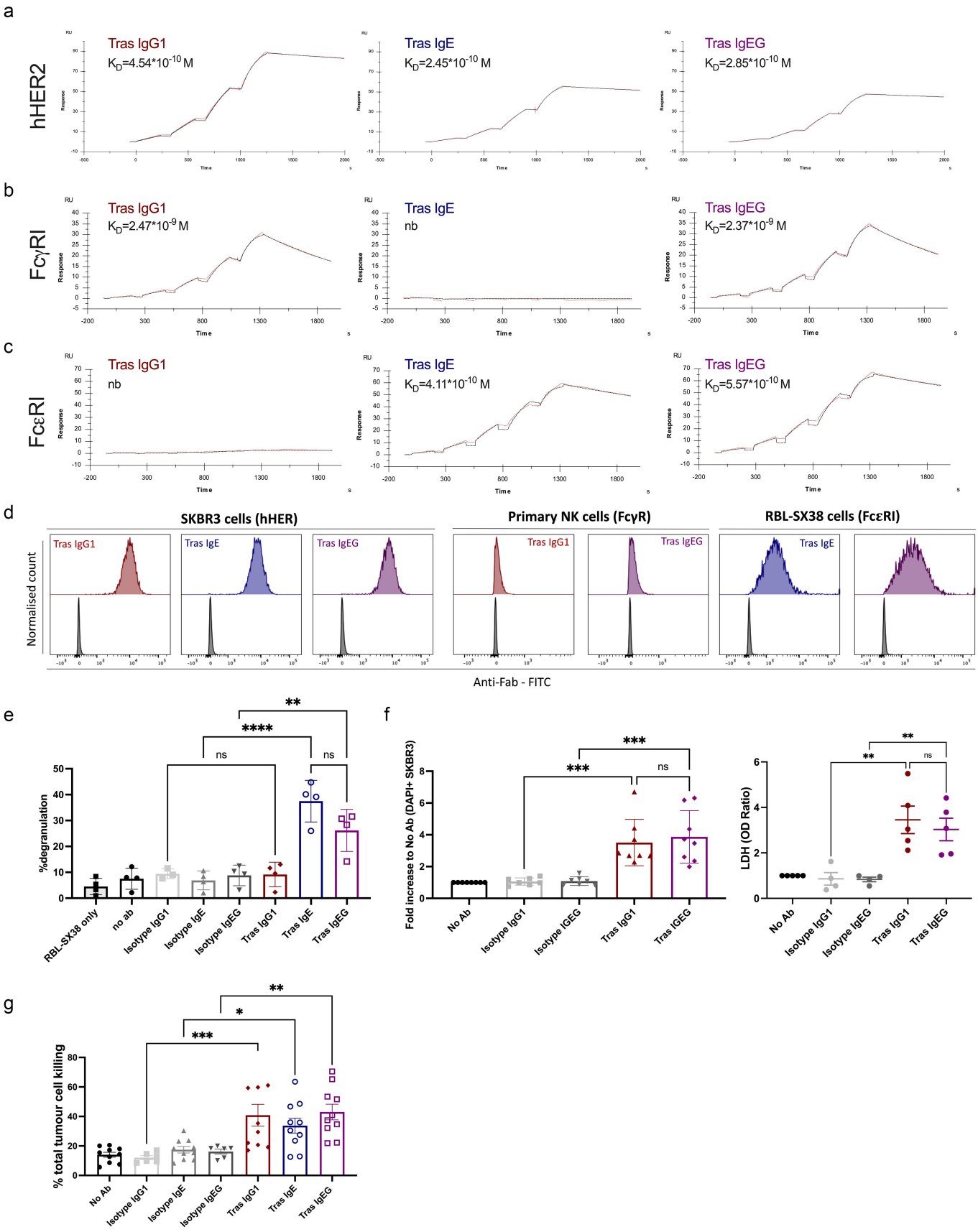

Figure 2. Affinity and in vitro functionality of Tras IgEG. (a-c) SPR sensorgrams and calculated affinities (KD) of Tras IgG1, IgE and IgEG binding to antigen (hHER2, A) and to high affinity fc receptors (hFcγri, B; hFcεri, C) (nb = no binding). (d) flow cytometric histograms depicting cell surface binding of Tras IgG1 (red), IgE (blue) and IgEG (purple) (52.6 nM) to hHER2-expressing SKBR3 cells, of IgG1 and IgEG to hFcγr+ primary NK cells; and of IgE and IgEG to hFcεri+ RBL-SX38 cells (top row). Matched unspecific isotype mAbs (SKBR3) or secondary antibody-only (primary NK and RBL-SX38 cells) used as background controls are shown in gray (bottom row). (e) Tras IgE and IgEG, but not IgG1 induce degranulation of RBL- S×38 cells upon target-specific crosslinking by HER2-expressing SKBR3 cells ($n = 4$). (f) Tras IgG1 and IgEG mediate ADCC against SKBR3 cells by primary human NK cells measured both by flow cytometry, by increase in dead cells (DAPI+ SKBR3) ($n = 8$) and by increase in lactate-dehydrogenase (LDH) in co- culture supernatant ($n = 5$). (g) tras IgG1, IgE and IgEG mediate tumor cell killing of SKBR3 cells by human PBMCs ($n = 10$). Mean ± SD (E) or SEM (f-g) are shown. One way ANOVA (E-G). *$p \le 0.05$; **$p \le 0.01$; ***$p \le 0.001$; ****$p \le 0.0001$; ns non-significant.

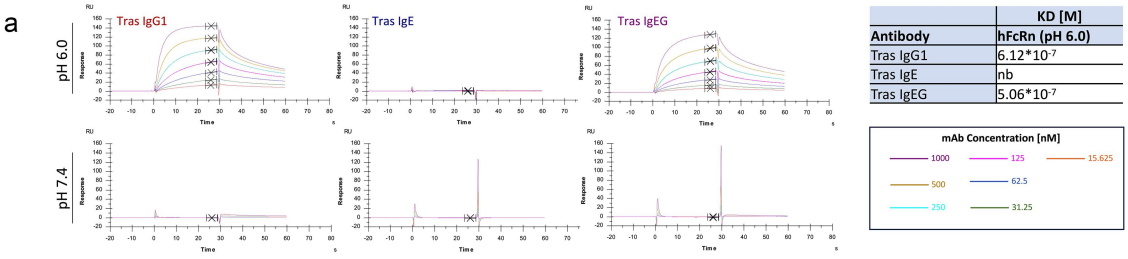

Antibody	KD [M] hFcRn (pH 6.0)
Tras IgG1	$6.12*10^{-7}$
Tras IgE	nb
Tras IgEG	$5.06*10^{-7}$

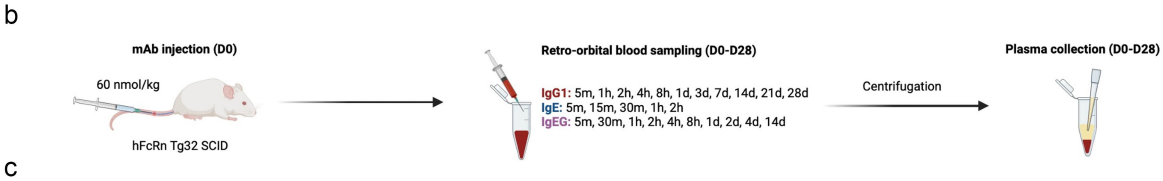

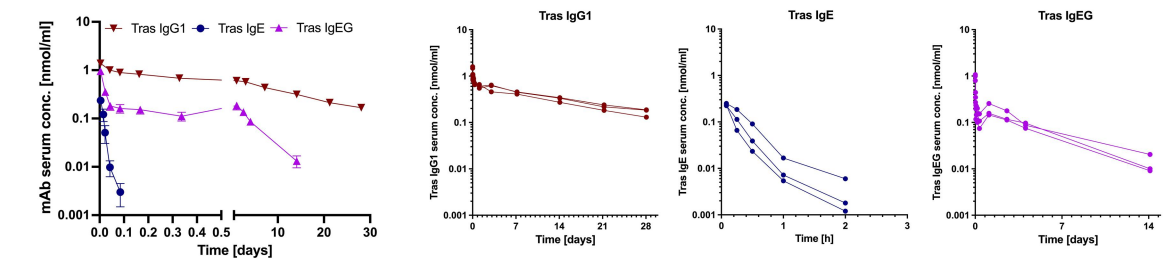

	Half-Life [days]	Half-Life [h]	Clearance [mL/h/kg]	Cmax [nmol/mL]	AUC [nmol-days/mL]	Volume of Distribution [mL/kg]
Tras IgG1	14.13	339	0.220	1.38	9.8	106
SEM	1.02	25	0.020	0.16	0.4	3
Tras IgE*	0.008	0.183	577	0.24	0.003	152
SEM	0.000	0.007	113	0.01	0.001	31
Tras IgEG	3.42	82	1.705	0.96	1.1	200
SEM	0.17	4	0.205	0.08	0.1	16

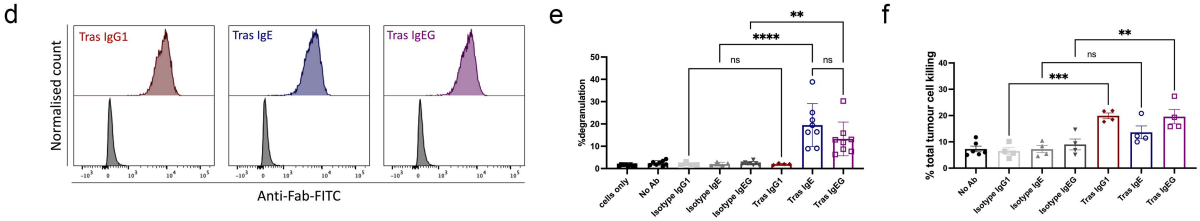

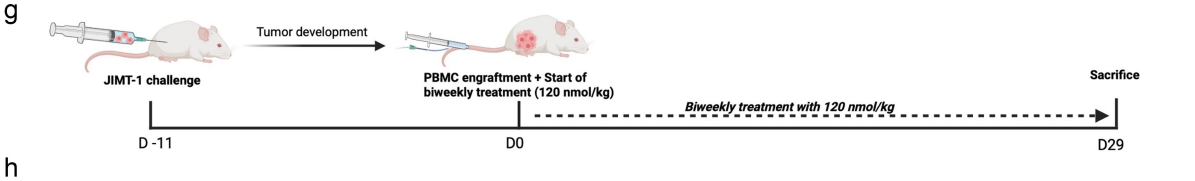

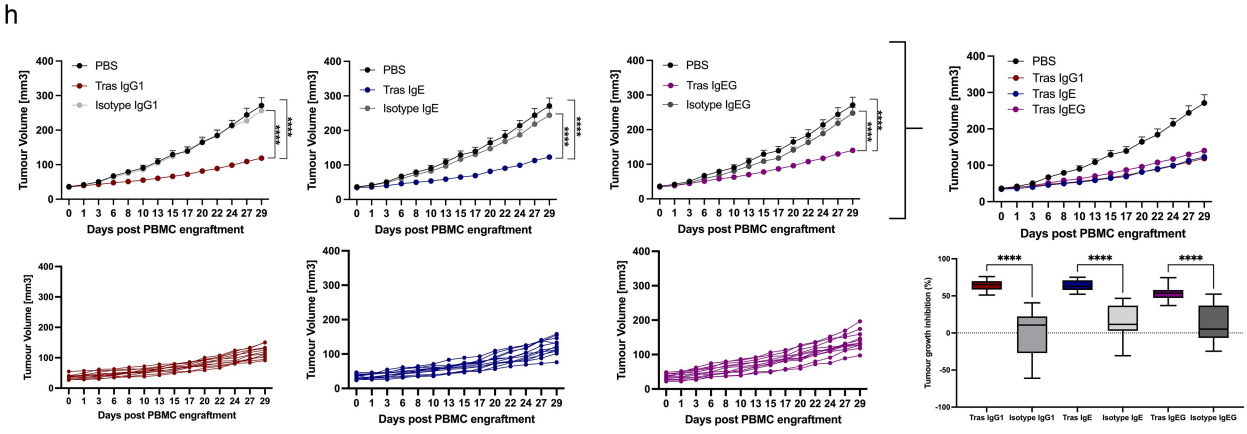

Figure 3. In vivo properties of the anti-HER2 targeting Tras IgEG. (a) SPR sensorgrams and calculated affinities (KD) of Tras IgG1, IgE and IgEG binding to hFcrn at pH 6.0 and pH 7.4 (nb = no binding). (b) schematic of study design to determine pharmacokinetics of Tras IgG1, IgE and IgEG in hFcrn transgenic mice. (c) serum concentration of Tras IgG1, IgE and IgEG in hFcrn mice over time, as determined by ELISA ($n = 3$) (left: mean ± SEM; right: individual mice; lower table: calculated PK parameters.

IgE or IgEG (Figure 3g). Significant tumor growth restriction was observed following treatment with all three Tras constructs in contrast to their corresponding isotype controls (Figure 3h). There were no significant differences in efficacy between the three trastuzumab isotypes at these high doses (approx. 50–60% tumor growth inhibition (TGI)). Furthermore, no overt adverse events were observed following treatment with any of the Tras constructs (Suplementary Figure S3E).

IgEG retains its characteristics when formatted with proprietary anti-HER2 variable domains and is efficacious at low doses

Having validated the IgEG modality in a trastuzumab format, we sought to investigate whether these characteristics would be retained in an IgEG construct incorporating alternative variable domains. For this purpose, we selected our proprietary anti-HER2 antibody 26, which was shown to be efficacious against HER2-expressing tumors in an IgE format.[21] Following production and purification, the IgG1, IgE and IgEG of antibody 26, displayed the expected size and purity (Supplementary Figure S4A and S4B). Binding affinities of 26 IgG1, IgE and IgEG to hHER2, FcγRI, FcεRI and FcRn, as determined by Octet, were in the expected range and concordant with the Tras isotypes (Supplementary Figure S4C). Upon crosslinking with JIMT-1 cells, 26 IgE and 26 IgEG induced significant RBL-SX38 cell degranulation, and 26 IgG1 and 26 IgEG mediated significant ADCC by the primary NK cells (Supplementary Figure S4D), thus confirming *in vitro* dual-isotype functionality. In agreement with the pharmacokinetic profile of Tras IgEG, the serum half-life of 26 IgEG in FcRn humanized mice was elongated as compared to 26 IgE (Figure 4a, Supplementary Figure S4E, study design as per Figure 3b). Employing the JIMT-1 human breast cancer xenograft mouse model, we assessed the efficacy of 26 IgG1, IgE and IgEG at biweekly doses of 12, 60 or 120 nmol/kg *in vivo* (Figure 4b). At the lowest dose (12 nmol/kg), statistically significant tumor growth restriction was observed for 26 IgEG and 26 IgE treatment (approx. 30–40% TGI), whereas 26 IgG1 was not efficacious at this dose. At higher doses (60 and 120 nmol/kg) all three isotypes significantly inhibited tumor growth to a similar extent (Figure 4c-e; Supplementary Fig. S4F-H). No overt adverse events were observed for any of the 26 constructs (Supplementary Figure S4G).

These data highlight that IgEGs retain their unique properties when constructed with different Fv regions and that they show promising *in vivo* efficacy against HER2+ tumors, even at low doses.

IgEGs show no indication of ex vivo basophil activation in human blood

Having demonstrated that IgEGs possess the intended dual-isotype functionality, we considered whether they could bind to FcγR and FcεR simultaneously. To investigate potential simultaneous Fc-receptor binding, a sandwich SPR approach was used. There was evidence of low simultaneous binding of Tras IgEG when initially bound to FcεRI, followed by FcγRI binding. There was negligible simultaneous binding when IgEG was initially bound to FcγRI (Figure 5a). Based on these findings, an *ex vivo* whole-blood basophil activation test (BAT) was used to determine whether the IgEG construct alone could potentially trigger a type I hypersensitivity reaction by antigen-independent crosslinking of Fc receptors on immune cells (Figure 5b). Activation, assessed by increased CD63 expression by $CCR3_{high}$-SCC_{low} human basophils, was observed upon stimulation by three positive immune stimuli (anti-FcεRI, anti-IgE and fMLP), but not by Tras IgEG, or its IgG1 and IgE counterparts, in any of the human samples tested (Figure 5c,d; 10 hVs).

These data provide preliminary indication that IgEGs do not pose a material risk for triggering type I hypersensitivity in humans.

Discussion

Monoclonal antibodies directed to cancer-associated antigens elicit target-specific anti-tumor effects and have been implemented as standard of care for several malignancies.[7] Typically, approved mAbs are of the IgG class,[1] specifically of the IgG1 subtype when activation of the immune system is desired. While anti-cancer IgG1 mAbs have improved patient outcomes in some cancers, responses are variable between patients and between cancers.[4,8] The immunosuppressive environment in the TME,[28–30] especially associated with significant upregulation of FcγRIIb,[6] may dampen immune responses mediated by Fc-unmodified and Fc-modified IgG1 mAbs. Application of other isotypes for anti-cancer mAb therapies, such as IgE, with their ability to activate a distinct arm of the immune system, may be needed to overcome these limitations. To that end, we have previously reported significant Fc-mediated anti-tumor functions of IgE *in vitro*,[16,17,22] anti-tumoral efficacy *in vivo*,[18–21] and a good safety profile and signs of early

*terminal half-life could not be determined; half-life was calculated manually using all data points). (d) histograms showing cell-surface binding of Tras IgG1 (red), IgE (blue) and IgEG (purple) to herceptest 2+ JIMT-1 breast cancer cells (top row). Matched unspecific isotype mAbs used as background controls are shown in gray (bottom row). (e) degranulation of RBL-SX38 cells by both Tras IgE and IgEG, but not IgG1, in the presence of HER2-expressing JIMT-1 cells ($n = 4$). (f) Antibody-mediated tumor cell killing of JIMT-1 cells by human PBMCs ($n = 4$). (g) design of efficacy study in immunodeficient mice challenged with JIMT-1 cells and engrafted with human PBMCs. (h) top: significant tumor growth restriction compared to the respective nonspecific isotype control was observed for Tras IgG1, IgE and IgEG, with no significant differences observed between the three constructs. Bottom: growth curves for individual animals for each construct ($n = 12$). Bottom far right: calculated tumor growth inhibition (%), as compared to respective isotype controls. Mean ± SD (E) or SEM (C, F, H) are shown. One-way ANOVA (E, F, H: % tumor growth inhibition). Two-way ANOVA (H: tumor volume; full statistical results shown in supplementary Figure S3f). *$p \le 0.05$; **$p \le 0.01$; ***$p \le 0.001$; ****$p \le 0.0001$; ns non-significant.

a

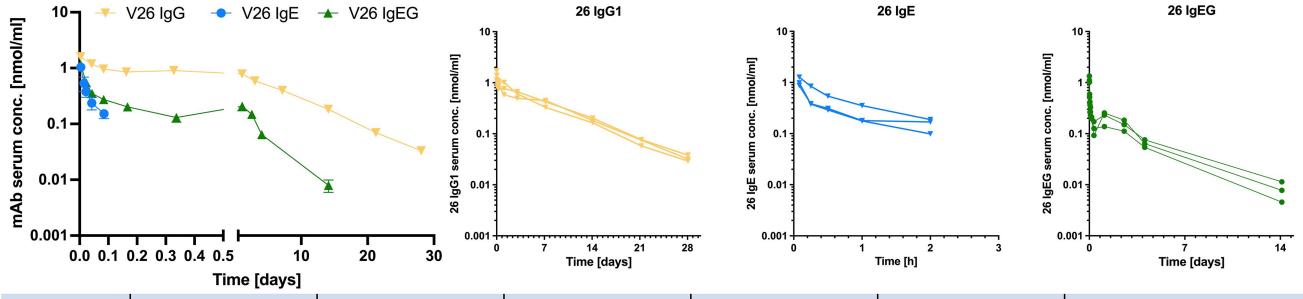

	Half-Life [days]	Half-Life [h]	Clearance [mL/h/kg]	Cmax [nmol/mL]	AUC [nmol-days/mL]	Volume of Distribution [mL/kg]
V26 IgG1	5.95	143	0.367	1.60	7.61	76
SEM	0.28	7	0.011	0.11	0.41	4
V26 IgE*	0.045	1.077	67	1.04	0.026	103
SEM	0.009	0.210	11	0.10	0.004	23
V26 IgEG	2.80	67	1.897	1.15	1.00	183
SEM	0.15	4	0.245	0.12	0.09	18

b

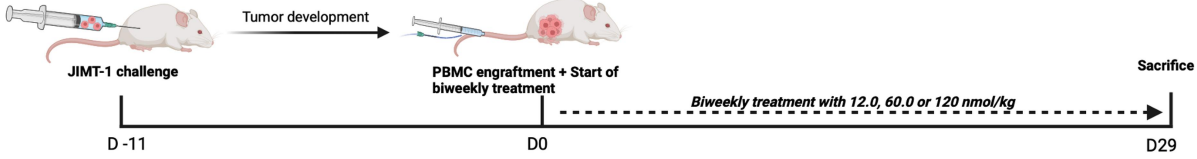

c

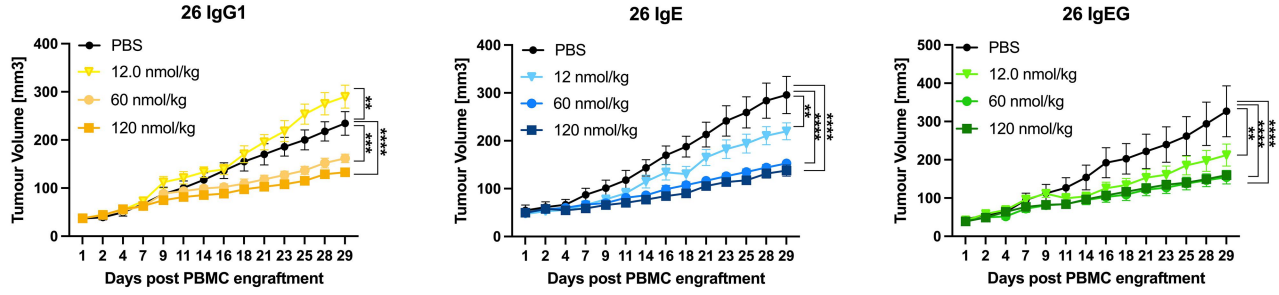

d

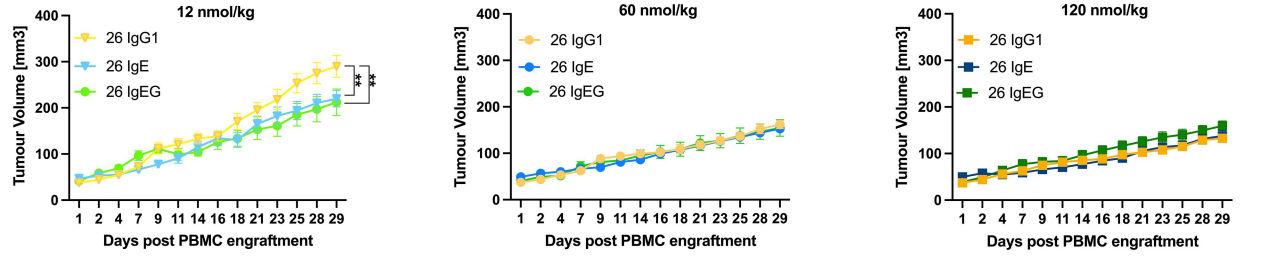

e

	Tumour growth inhibtion (Mean ± SEM)		
Dose (nmol/kg)	**26 IgG1**	**26 IgE**	**26 IgEG**
12	-27.6 ± 11.01	28.3 ± 5.60	39.7 ± 10.37
60	37.2 ± 3.72	58.1 ± 2.04	59.6 ± 5.23
120	51.6 ± 3.21	62.3 ± 4.47	57.2 ± 3.80

Figure 4. In vivo properties of the anti-HER2 targeting 26 IgEG: (a) serum concentration of 26 IgG1, IgE and IgEG in hFcrn mice over time, as determined by ELISA ($n = 3$; left: mean ± SEM; right: individual mice; lower table: calculated PK parameters. *terminal half-life could not be determined; half-life was calculated manually using all data points). (b) design of dose–response study in immunocompromised mice challenged with JIMT-1 human breast cancer cells and engrafted with human PBMCs. (c) significant tumor growth restriction, compared to untreated animals, was observed for 26 IgE and IgEG at all three doses, but only at the two higher doses for IgG1 ($n = 5$–6). (d) significantly greater tumor growth restriction by 26 IgE or IgEG, in comparison to IgG1, at the lowest dose. No differences between constructs were observed at higher concentration (growth curves for individual animals treated with each 26 construct are shown in supplementary Figure 4E). (e) calculated tumor growth inhibition (%) of the three 26 constructs at 12, 60 and 120 nmol/kg. Mean ± SEM (A, C-E) are shown. Two-way ANOVA (C, D; full statistical results shown in supplementary Figure. 4 h). *$p \leq 0.05$; **$p \leq 0.01$; ***$p \leq 0.001$; ****$p \leq 0.0001$; ns non-significant.

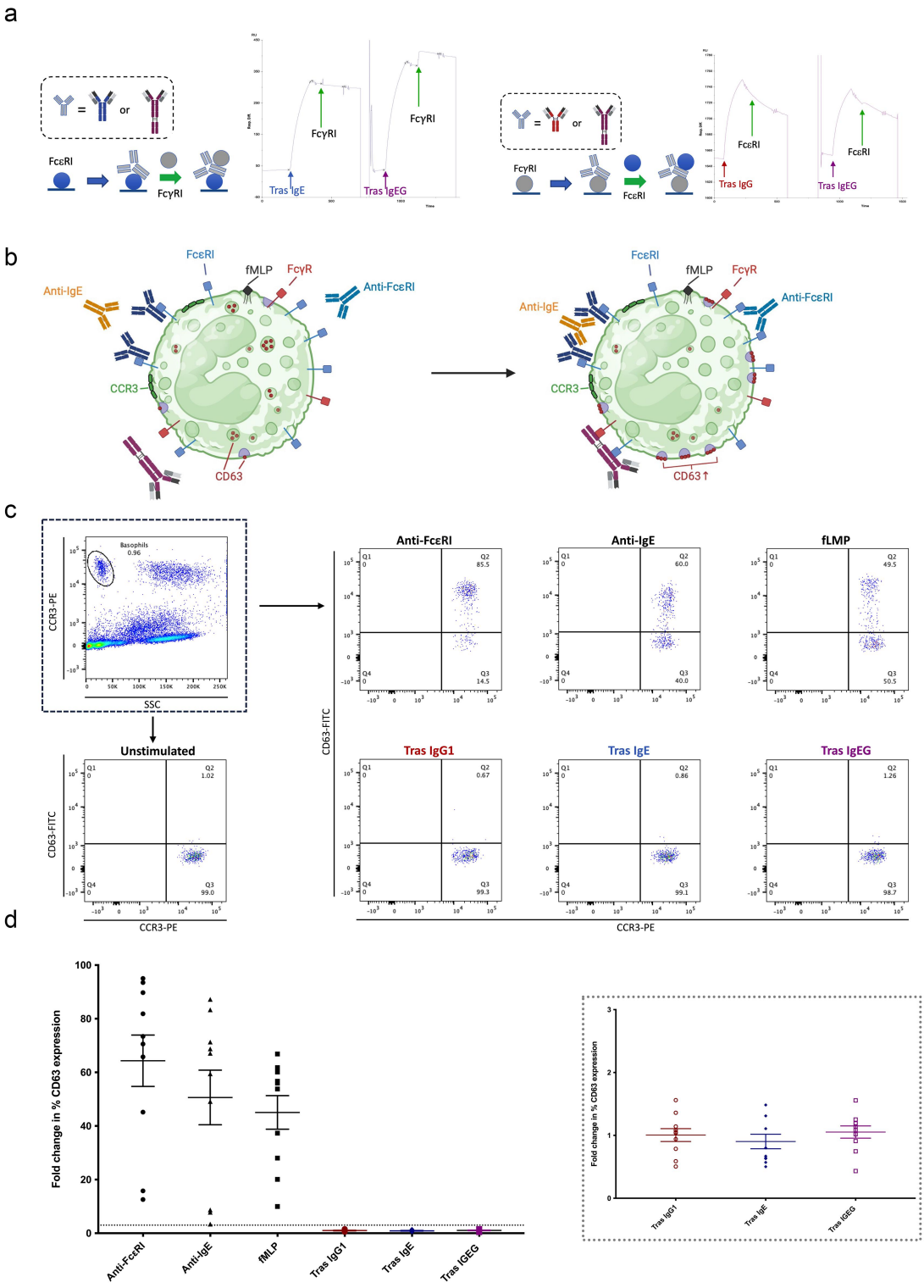

Figure 5. Evaluation of simultaneous FcγRI and FcεR binding and basophil activation. (a) SPR analyses to evaluate potential simultaneous binding of IgEG to FcγRI and FcεRI. The two approaches used are shown in schematics to the left of the sensorgrams. (b) schematic of basophil activation test (BAT) with binding of positive immune stimuli (anti-FcεRI, anti-IgE and fMLP), and potential simultaneous binding of IgEGs to fc γ and ε receptors, leading to crosslinking and basophil activation, as measured by cell surface CD63 upregulation. (c) flow cytometric gating strategy and representative flow cytometry plots for positive immune stimuli, and Tras IgG1, IgE and IgEG antibodies in the BAT. (d) basophil activation was triggered upon ex vivo stimulation of unfractionated human blood samples with positive immune stimuli, but not by Tras IgG1, IgE or IgEG ($n = 10$). Mean ± SEM are shown.

efficacy of an IgE in ovarian cancer patients.[23] Here, we aimed to improve efficacy further by combining the beneficial traits of IgG1 and IgE in a single antibody molecule. Given the often-critical role that specific epitopes play in therapeutic antibody performance,[31] IgEGs have the unique advantage of being able to direct both IgE and IgG immune effector functions against the same epitope on a tumor-associated antigen. By obviating combination therapy and

thereby eliminating issues around epitope competition, IgEGs may enable enhanced potency, simplified dosing regimens[32] and lowered treatment costs.[33,34]

In this study, we have demonstrated that stable IgEGs can be easily expressed in mammalian cells and purified to a high standard using conventional Protein A affinity chromatography and SEC-HPLC polishing. Biochemical characterization of the two anti-HER2 IgEGs confirmed that binding to hHER2, FcγRI and FcεRI is comparable to their respective IgG1 and IgE counterparts. *In vitro*, IgEGs triggered FcεR-mediated degranulation of RBL-SX38 cells to a similar level as the corresponding anti-HER2 IgE isotype. IgEGs also mediated significant FcγR-mediated ADCC by NK cells comparable to their counterpart IgG1. In contrast to IgEGs, IgE is only able to trigger FcεR-mediated immune functions and IgG1 only triggers FcγR-mediated immune functions.

An attribute of IgG that is not shared by IgE is its ability to bind in a pH-dependent manner to the neonatal Fc receptor (FcRn).[26] This interaction contributes to the elongated serum half-life of IgG.[3] The affinity of the anti-HER2 IgEGs to FcRn at pH 6.0 was found to be equivalent to that of the corresponding IgG1 and, as with IgG1, binding to FcRn was absent at physiological pH. This resulted in the significant *in vivo* elongation of serum half-life of IgEGs compared with IgE in a human FcRn transgenic mouse model. However, despite having equivalent affinities to FcRn, the serum half-life of the IgEGs was not extended to the degree seen with the corresponding IgG1. A disparity in *in vivo* pharmacokinetic profiles has been described for IgG1s with identical Fc but unique Fab/Fv regions. These disparities have been proposed to stem from differences in the distribution of charges on the Fv regions which may contribute to interactions with FcRn.[35] However, in this study, the Fvs of the two IgEGs are the same as those of the corresponding IgG1 and they are thus unlikely to be responsible for this PK difference.

Differences in glycosylation levels between IgEG and IgG1 may contribute to differences in clearance from the circulation and the consequent differences in PK. The impact of glycosylation on blood clearance has previously been demonstrated for IgA: removal of glycans that decorate IgA resulted in prolonged serum half-life *in vivo* without negatively impacting the tumor-targeting efficacy of the antibody.[36,37] Further work is thus required to understand the determinants of the PK differences between IgEG and IgG1.

Importantly, in this study, we demonstrated the efficacy of two anti-HER2 IgEGs in a medium/low HER2 (Herceptest 2+) breast cancer xenograft model. Tras IgEG showed comparable tumor growth inhibition to Tras IgG1 and Tras IgE upon biweekly administration at 120 nmol/kg. With our proprietary anti-HER2 mAb 26, we not only corroborated this result at 120 nmol/kg but also showed that 26 IgEG and 26 IgE statistically significantly reduced tumor burden at a low dose of 12 nmol/kg biweekly, at which dose and schedule 26 IgG1 was ineffective. The ability of an IgEG to show dual-isotype functionality as demonstrated *in vitro* did not lead to improved tumor growth reduction compared to IgE in this model.

Our findings highlight the promising anti-tumor potential of combining IgE and IgG1 functionality in a hybrid antibody format but also exemplify the complexity and challenges associated with engineering novel modalities like IgEG. A key limitation is the lack of *in vivo* models, that accurately represent IgG and IgE biology simultaneously, thereby hampering the assessment of the full therapeutic potential of IgEG. While existing models may be informative for comparing antibodies of the same isotype, they do not support a balanced comparison across different isotypes, due to selective enrichment of certain immune cell types. As a platform to assess initial efficacy, we used an immunodeficient human xenograft mouse model engrafted with human PBMCs. While these models provide circulating immune effector cells such as monocytes and NK cells for IgE and/or IgG engagement, respectively, they cannot adequately recapitulate the full range of human immune responses. Limitations include transient and incomplete immune cell engraftment and a lack of tissue-resident immune cells in appropriate anatomical locations.[38] Although human hematopoietic stem cell-engrafted models provide more durable and improved reconstitution of the human immune system, these models are also characterized by over- and/or underrepresentation of specific cell types.[39] Thus, the anti-tumor activity of individual antibody isotypes may not be appropriately reflected in these models and would have equally not provided a comprehensive assessment of IgEG's therapeutic potential.

Notably, most models, including the one used in this study, do not support adequate development of human mast cells.[39,40] These FcεRI-high expressing cells are not only important mediators of IgE-driven responses but may also be enriched in many TMEs.[41] Activation of mast cells via the IgE-Fc region of IgEG may be crucial to its mechanism of action; thus, their absence may lead to a significant underestimation of IgEG's anti-tumor activity.

These limitations highlight the need for next-generation humanized *in vivo* models that allow for broad and more physiologically balanced human immune cell representation. This is particularly pertinent for evaluating the efficacy of complex hybrid antibodies such as IgEG. The development of such models would be instrumental in driving innovation for complex therapeutic modalities. They would allow a more comprehensive assessment of the full potential of IgEG and a more accurate, unbiased comparison of IgG, IgE and IgEG effector mechanisms.

Aside from the above, determining synergistic functionality for IgEG proved to be challenging *in vitro*. While we demonstrated that IgEG can engage immune effector cells via FcεR and FcγR using conventional *in vitro* assays, these did not allow assessment of potentially enhanced functionality through synergism. Such synergistic effects may potentially be engendered within the TME. The ability of IgG1 to activate peripheral immune cells, such as NK cells is well-established. However, within the TME IgG1-mediated effector activity is often limited due to the prevalence of immune cells such as M2-like tumor-associated macrophages (TAMs) with high expression levels of the inhibitory receptor FcγRIIb.[6,42] In contrast, the IgE domain of IgEG may engage with TAMs and repolarize FcγRIIb^{high} M2-like TAMs toward an M1-like phenotype[15,18,43] with reduced FcγRIIb expression.[42] These repolarized TAMs may then be effectively engaged by the IgG1-domain of IgEG, thus mediating tumor cell killing and release of pro-inflammatory cytokines. This may in

turn promote enhanced infiltration of cytotoxic $CD8^+$ T-cells and a pro-inflammatory response. Additionally, IgE engagement has been associated with a reduction of regulatory T cells (Tregs) within the TME, resulting in a favorable effector T cell-to-Treg ratio.[20,43] Thus, the IgEG modality may harbor the potential to overcome immunosuppressive barriers within the TME and leverage the anti-tumoral activity of both IgG1 and IgE. Future studies may include the development and application of novel models that better mimic the immune microenvironment and complexity of the TME to evaluate potential synergistic IgEG effector functions *in vitro*.

While IgEG may activate the immune system within the immunosuppressive TME through FcεR engagement, its unmodified IgG1 Fc region may still engage FcγRIIb, thereby potentially limiting its maximal anti-tumor activity. Therefore, future studies may explore fine-tuning of IgG1 Fc functions of IgEG through Fc engineering. For example, an Fc-engineered version of IgEG with reduced affinity to FcγRIIb and enhanced affinity for an activatory FcγR may optimize IgE-IgG1 synergistic anti-tumor activity within the TME, and thus improve overall efficacy.

A consideration as to the viability of IgEGs to progress into human trials requires an assessment as to whether antigen-independent crosslinking of Fc receptors on immune cells through simultaneous Fcε- and Fcγ- receptor binding might occur. Using SPR, we observed very low levels of simultaneous Fcε and Fcγ-receptor binding, especially when the IgEG encountered FcγRI before FcεRI where simultaneous binding was negligible. Moreover, in an *ex vivo* BAT performed using whole human blood, the IgEGs did not lead to activation of basophils. This indicates a lack of inherent antigen-independent crosslinking and is a first indication of safety for a therapeutic IgEG.

In summary, we engineered a novel IgE-IgG1 hybrid antibody that expresses well in mammalian cells and can be readily processed to high levels of purity. IgEGs possess levels of stability and solubility that are similar to their IgE and IgG counterparts. Furthermore, we showed that IgEGs were able to stimulate a broader range of immune functions compared to either an IgG or an IgE and have an enhanced PK profile compared to IgE. No obvious safety concerns were identified in an *ex vivo* basophil activation assessment and IgEGs were shown to be capable of generating statistically significant and reproducible anti-tumor activities *in vivo*. Our findings demonstrate that an IgEG could represent a novel and potent therapeutic modality with applicability in the treatment of solid tumors.

Materials and methods

Ethical statement

The research presented here complies with all ethical regulations. Human blood samples were collected under REC numbers 09/H0804/45 and 16/LO/0366 approved by Guy's Research Ethics Committee, Guy's and St. Thomas' NHS Trust or obtained from the UK National Health System Blood and Transplant (NHSBT) system using anonymous donor leukocyte cones following provision of written, informed consent. Animal studies and procedures were performed following all relevant ethical regulations.

Cell culture and isolation

Cells were maintained at 5% CO_2 and 37°C. SKBR3 (ATCC HTB-30) and JIMT-1 (DSMZ ACC 589) cells were cultured in complete DMEM (10% fetal bovine serum (FBS), penicillin (5,000 U/ml), streptomycin (100 µg/ml)). The rat basophilic cell line RBL-SX38 (carrying the human FcεRα transgene, kindly provided by Prof. Jean-Pierre Kinet) was cultured using complete RPMI1640 (10% FBS, penicillin (5,000 U/ml), streptomycin (100 µg/ml)), with added G418 as selection. Peripheral blood mononuclear cells (PBMCs) of healthy volunteers were isolated using Ficoll-Paque as previously described.[1] Primary NK cells were isolated using the RosetteSep™ Human NK Cell Enrichment Cocktail (Stemcell) following the manufacturer's instructions. After isolation, NK cells were either used immediately for binding experiments or maintained overnight in RPMI1640 containing 10% human AB serum.

Antibody production and biophysical characterisation

Production and purification

All HER2-targeting mAb isotypes and unspecific isotype controls were expressed using stably transfected CHO-K1 cells. Antibodies were purified using an affinity column, followed by a SEC-HPLC polishing step. A protein A matrix was used for purification of IgG1 and IgEG isotypes, whereas a -CaptureSelect™ IgE matrix was used for purification of IgE isotypes. Purified mAbs in PBS 7.4 were tested for endotoxin and subsequently stored at 4°C.

Sodium dodecyl sulfate polyacrylamide electrophoresis

Protein samples for SDS-PAGE were prepared using BioRad 4× LDS Sample buffer with and without 1 µL mercaptoethanol, for reduced and non-reduced conditions, respectively. Samples were heated for 5 min at 95°C and loaded onto a 4–15% Mini-PROTEAN® TGX™ Precast (Bio-Rad) with 1× Tris-Glycine SDS as running buffer. Constant voltage of 120 V was applied for 1 h and gels subsequently stained using InstantBlue® Coomassie Protein Stain.

Analytical size-exclusion high performance liquid chromatography

Proteins were analyzed for monodispersity on a Vanquish Horizon UHPLC (ThermoFisher Scientific) using an AdvanceBio SEC size exclusion column (300 Å, 7.8 × 150 mm, 2. 7 µm, Agilent). 5 µg of mAb at 5.26 µM or molecular weight standard (Agilent ReadyCal Red, Supplementary Figure S1A) were loaded onto the column. The run was performed in 0.1 M sodium phosphate buffer + 0.01% sodium azide (pH 7.0) at a flow rate of 0.35 mL/min for 10 min (column temperature 30°C). Eluted proteins were detected at 280 nm with a data collection rate of 5.0 hz. Data was generated and processed in Chromeleon version 7.3.1.

Stability assessments

Melting profiles and temperatures of the respective mAbs were determined using DSF. Briefly, each respective mAb (final conc. 10 µM) was run in triplicate with added SyproOrange (5×) on a BioRad Connect CFX machine. Fluorescence was recorded from 20 to 95 °C at increments of 0.2°C.

To determine the freeze-thaw stability of the IgEG modality, aliquots of Tras IgEG stored for 6 weeks at 4°C were frozen for 24 hours at either −20 or −80°C. Following thawing, monodispersity was analyzed by SEC-HPLC as described above. Retention of binding affinity to hHER2 was assessed by SPR as described below.

Antibody affinity and cell-surface binding

Affinity measurements by surface plasmon resonance

The binding kinetics of Tras IgG1, IgE and IgEG to hHER2, FcγRI, FcεRI, C1q and FcRn were determined using a Biacore T200 instrument (Cytiva, USA) at 25°C. Sensorgrams were corrected with appropriate blank references and analyzed using Biacore T200 Evaluation Software V 2.0.1.

A Fab capture approach was used to determine affinities to hHER2. Briefly, a mixture of anti-kappa and anti-lambda mAb (Human Fab Capture kit, Cytiva UK) was immobilized onto a CM5 chip. Purified antibodies were diluted to 52.63 nM and captured to a R_{max} of 45 at 10 µl/min. HBS-EP+ (10 mm HEPES, pH 7.4, 150 mm NaCl, 3 mm EDTA and 0.05% surfactant *p*-20) with added 1 mg/ml bovine serum albumin (BSA) was used as running buffer. Recombinant hHER2 was applied at four concentrations (1.11 nM, 3.33 nM, 10 nM and 30 nM) with an association and dissociation time of 240 s and 600 s, respectively. Subsequently, chips were regenerated by washing twice with 10 mm glycine-HCl, pH 2.1.

Measurements for FcγRI and FcεRI were performed using a CM5 chip coupled with an anti-His antibody (His Capture kit, Cytiva UK) and HBS-P+ (10 mm HEPES, 150 mm NaCl and 0.05% v/v Surfactant P20) as running buffer. hFcγRI (Sino Biological) or hFcεRI (R&D Systems) was captured to 30 RU at 10 µL/min. Purified antibodies (3-fold dilution, 33.33 nM – 0.411 nM) were flowed over the chip at 30 µL/min with an association and dissociation time of 200 s and 600 s, respectively. Chips were regenerated by washing twice with 10 mm glycine-HCl, pH 1.5.

For affinity measurements to C1q, a protein A capture sensor chip (Cytiva, UK) with HBS-EP+ as running buffer was used. Purified antibodies were diluted to 1 µg/ml in running buffer and captured at 10 µl/min. C1q (QuidelOrtho) protein (3-fold dilution, 120 nM – 4.444 nM) was flowed over the chip at 30 µL/min with an association and dissociation time of 90 s and 120 s, respectively. Chips were regenerated by washing twice with 10 mm glycine-HCl, pH 1.5.

Binding kinetics to hFcRn were determined by coupling CM5 chips with recombinant hFcRn. Phosphate-buffered saline (PBS) + 0.05% Tween 20 (pH 6.0 or pH 7.4) containing an additional 150 mm NaCl was used as running buffer. The respective purified antibodies (two-fold dilution from 1000–15.625 nM) were flowed over the chip at a flow rate of 30 µL/min, with an association and dissociation time of 30 s. Chips were regenerated with 100 mm Tris, pH 8.0.

Affinity measurements by bio-layer interferometry

Bio-layer interferometry (BLI) experiments were performed on the Octet R8 machine (Sartorius). Ligands (ACROBiosystems) were immobilized onto Streptavidin SA biosensors (Sartorius) at the following concentrations: hHER2-biotin (0.20 µg/ml), hFcεRI-biotin (0.25 µg/ml), hFcγRI-biotin (0.25 µg/ml), and hFcRn (0.125 µg/ml). The following experimental setup was used: wash (60 s), load (600 s), wash (60 s), baseline (30 s), association (180 s), dissociation (variable time, until at least 5% ligand dissociated). Wash and baseline steps were performed in different wells. For the dissociation the sensor was re-dipped into the baseline wells. Association was performed using a 5-fold 3-times dilution series of the respective antibodies with the following starting concentrations: 100 nM (HER2, FcεRI, and FcγRI), 300 nM (FcRn). PBS pH 7.4 with 0.05% (v/v) Tween-20 (PBST) was used for all sample preparation and for assay steps. For FcRn, runs were performed in 50 mm sodium phosphate, 150 mm sodium chloride pH 6 with 0.05% (v/v) Tween-20. The second wash, baseline, association, and dissociation steps were performed in pH 6 buffer. Runs were set up using 96-well plates shaking at 1000 rpm at 30°C. Data was fit using the Octet kinetics analysis software using a global fit (1:1 for FcεRI and FcγRI and 1:2 bivalent analyte for HER2 and FcRn).

Simultaneous receptor binding assessment

Potential binding of IgEG to FcγR and FcεR simultaneously was assessed using SPR. FcγRI (Sino Biological) or FcεRIα (R&D Systems) were immobilized onto a CM5 chip by standard amine coupling. Antibodies were injected manually at 50 nM and captured either through FcγRI or FcεRIα. This was followed by injection 50 nM of either FcεRIα or FcγRI, respectively, to assess simultaneous receptor binding. Chips were regenerated by washing with a 3 M $MgCl_2$ for 240 s.

Cell surface binding

For cell surface binding to SKBR3 (hHER2), JIMT-1 (hHER2) and RBL-SX38 (hFcεRI) cells, 1×10^5 cells were incubated for 30 min at 4°C with mAb (52.6 nM). Anti-Fab FITC (2 µg/ml, Invitrogen UK) was added as a detection antibody followed by a 30 min incubation at 4°C. Cells were washed with FACS buffer (PBS pH 7.2 + 2% FBS) between each step.

For cell surface binding to primary NK (FcγR) cells, the respective mAbs (52.6 nM) were incubated with an anti-Fab FITC detection antibody (2 µg/ml) for 20 min at 37°C prior to addition of NK cells. Subsequently, 1×10^5 primary NK cells were added and incubated for 30 min on ice, followed by two washes with fluorescence-activated cell sorting (FACS) buffer. All samples were acquired using a flow cytometer (Fortessa, Becton Dickinson). Analysis was performed using FlowJo™software.

In vitro and ex vivo assays

FcεRI-mediated degranulation assays

RBL-SX38 cells in complete RPMI were seeded at 1×10^4 cells/well in a sterile flat bottom 96-well plate and incubated

overnight at 37°C, 5% CO_2. Antibodies were added at a final concentration of 1.05 nM followed by a one-hour incubation at 37°C, 5% CO_2. The supernatant was discarded and followed by three washes with HBSS + 1% BSA (heat shock fraction). After addition of 3×10^4/well of target cells in HBSS + 1% BSA, plates were incubated for 30 min at 37°C, 5% CO_2. Subsequently, the supernatants were taken off and 20 µl diluted in 30 µl of HBSS + 1% BSA buffer in black flat bottom 96 well plates. 50 µl of β-hexoaminidase substrate (4-methylumbelliferyl N-acetyl-β-D-glucosaminide) were added and plates were incubated for 2 hours at 37 °C. The enzymatic reaction was stopped by the addition of 100 µl of 0.5 M Tris-HCl buffer. Fluorescence was measured at 350 nm excitation and 450 nm emission using a Fluostar Omega microplate reader (BMG Labtech).

Tumour cell killing assays

Tumour cell killing assays were performed according to Bracher et al.[44] Briefly, the day before the experiment, target cancer cells were stained with carboxyfluoroscein succinimidyl ester. The next day freshly isolated PBMCs or primary NK cells from healthy volunteers were added at an effector to target cell ratio (E:T) of 10:1 or 5:1, respectively, to the stained target cells in the presence of antibody (final conc. = 26.32 nM). A no antibody control served as baseline. Samples were incubated for 3 hours at 37°C and 5% CO_2. Supernatants were taken off and cells were washed with FACS buffer prior to staining with 2 µg/ml of anti-human CD45 APC (BioLegend, UK) antibody for 30 min at 4°C. Samples were washed again and DAPI was added to the samples prior to acquisition using a flow cytometer (Fortessa, Becton Dickinson). Analysis was performed using FlowJo™software.

Supernatants from NK ADCCs were stored at −80°C and used in a CyQuant lactate dehydrogenase (LDH) Cytotoxicity Assay (Invitrogen, UK) following the manufacturer's instructions.

Ex vivo basophil activation test

BATs (Flow2 CAST® kit, Bühlmann Laboratories AG, Schönenbuch, Switzerland) using healthy volunteer peripheral blood were performed as previously described[19,45]Briefly, unfractionated whole blood was incubated with the provided stimulation buffer and anti-FcεRI (provided), anti-IgE antibody (Agilent Dako, Santa Clara, CA, USA) or fMLP (provided). *Ex vivo* stimulation with mAbs was performed at 19.5 nM. Samples were stained with the provided anti-CCR3-PE and anti-CD63-FITC staining cocktail and incubated at 37°C for 30 min in a 5% CO_2 incubator. After red blood cell lysis, samples were centrifuged, and cell pellets were resuspended in the provided acquisition buffer. Samples were acquired using a BD Fortessa.

In vivo studies

Pharmacokinetic in vivo studies

For PK studies, 10-week-old transgenic hFcRn+/mFcRn- Tg32 mice (B6.Cg-Fcgrttm1Dcr Prkdcscid Tg(FCGRT)32Dcr/MvwJ, Jackson Laboratory) were used. 60 nmol/kg of mAb were injected intravenously (i.v.) via the lateral tail vein. Blood samples (25 µL) into EDTA were taken retro-orbitally at multiple timepoints between 5 min and 28 days as indicated in Figure 3B and Supplementary figure S3C. Plasma was obtained by centrifugation 13,000 rpm for 5 min and diluted 1 in 10 in PBS + 50% glycerol prior to storing at −20°C. Serum levels of the respective mAbs were determined using an enzyme-linked immunosorbent assay (ELISA). For IgG and IgEG isotypes wells were coated with anti-human IgG (Mabtech MT145), serum was applied and IgG or IgEG detected using an alkaline phosphatase conjugated anti-human IgG (Mabtech MT78). To assess human IgE serum levels the Mabtech human IgE ELISA kit (3810-1A-6) was used. Pharmacokinetic parameters were determined using PK Solutions software (PK Solutions, Version 2.0 SUMMIT Research Services) using single dose, linear, noncompartmental analysis. The following parameters were analyzed: Area Under the Curve (AUC_{0-t}; µg-day/mL); Volume of distribution normalized to body weight (Vd; mL/kg), Clearance (CL; mL/h/kg) and Cmax (µg/mL). For IgG and IgEG molecules terminal half-life (h) from Vd was calculated using PK solutions software. For IgE it was not possible to calculate terminal half-life and therefore half-life was manually calculated using all data points.

In vivo efficacy studies

JIMT-1 cells were implanted subcutaneously at 1×10^7 in 50% Matrigel® on the rear dorsum of female NXG mice (Janvier Labs, France). Once tumors reached a volume of approximately 50 mm^3, mice were i.v. engrafted with 5×10^6 human PBMCs (day 0). The first dose (12, 60 or 120 nmol/kg) of each mAb was administered together with the PBMCs. All subsequent mAb doses were given i.v. without PBMCs on a biweekly schedule. For myeloid cell boost, FLT3 ligand was administered at 10 µg/mouse on days 0, 1 and 2. Tumors were measured three times a week and tumor size [mm^3] was calculated using the formula: $mm^3 = d2 \times (D/2)$ (d = smallest diameter of tumor; D = largest diameter of tumor).

Statistical analyses

Data are presented as mean ± Standard Deviation (SD) or Standard Error of the Mean (SEM) as indicated in the figure legends. GraphPad Prism was used to perform statistical analyses. Normality of data was evaluated using a Shapiro – Wilk normality test. Subsequently, appropriate statistical analyses were performed (One-way ANOVA and two-way ANOVA), and statistically significant differences are indicated in the graphs or additional tables were indicated. p values: *$p \leq 0.05$; **$p \leq 0.01$; ***$p \leq 0.001$; ****$p \leq 0.0001$.

Acknowledgments

We thank all volunteers who participated in this study. We thank all members of the Epsilogen team for work supporting antibody production and testing, and all Contract Research Organizations (CROs) that supported this study. This research was supported by the King's Health Partners Centre for Translational Medicine. The views expressed are those of the author(s) and not necessarily those of King's Health

Partners. The authors acknowledge the Advanced Cytometry Platform team, located in the R&D Department, Guy's and St Thomas' NHS Foundation Trust, Guy's Hospital, London, SE1 9RT.

Disclosure statement

No potential conflict of interest was reported by the author(s).

Funding

The work was supported by the Breast Cancer Now and Epsilogen Ltd .

ORCID

Melanie Grandits http://orcid.org/0000-0001-8143-8298
Sophia N. Karagiannis http://orcid.org/0000-0002-4100-7810
Heather J. Bax http://orcid.org/0000-0003-0432-4160

Author contributions

T.W., S.N.K., H.J.B, and K.F. designed and conceived the study. M.G., L.C.G.F.P., E.H., S.N.K., H.J.B., and K.F. developed the methodology. M.G., L.C.G.F.P., O.A., J.D., O.M., J.B., E.H. and H.J.B. acquired the data or helped with the data analysis. L.P. provided research management support. M.G., L.C.G.F.P., E.H., S.N.K., H.J.B., and K.F. discussed and interpreted the data, and wrote and edited the manuscript. E.H., S.N.K., H.J.B and K.F. supervised the study. All authors reviewed the manuscript and approved the submitted version. All authors agree to all manuscript contents, the author list and its order, and the author contribution statements.

Data availability statement

Source data are provided as a Source Data file.

References

1. The Antibody Society. Therapeutic monoclonal antibodies approved or in review in the EU or US. 2021. Accessed 2024 08 29.
2. Golay J, Introna M. Mechanism of action of therapeutic monoclonal antibodies: promises and pitfalls of in vitro and in vivo assays. Arch Biochem Biophys. 2012;526(2):146–153. doi: 10.1016/j.abb.2012.02.011.
3. Roopenian DC, Christianson GJ, Sproule TJ, Brown AC, Akilesh S, Jung N, Petkova S, Avanessian L, Choi EY, Shaffer DJ, et al. The MHC Class I-Like IgG receptor controls perinatal IgG transport, IgG homeostasis, and fate of IgG-fc-coupled Drugs1. J Immunol. 2003;170(7):3528–3533. doi: 10.4049/jimmunol.170.7.3528.
4. Levene AP, Singh G, Palmieri C. Therapeutic monoclonal antibodies in oncology. J R Soc Med. 2005;98(4):146–152. doi: 10.1177/014107680509800403.
5. Shafqat A, Omer MH, Ahmed EN, Mushtaq A, Ijaz E, Ahmed Z, Alkattan K, Yaqinuddin A. Reprogramming the immunosuppressive tumor microenvironment: exploiting angiogenesis and thrombosis to enhance immunotherapy. Front Immunol. 2023;14. doi: 10.3389/fimmu.2023.1200941.
6. Wu L, Xu Y, Zhao H, Zhou Y, Chen Y, Yang S, Lei J, Zhang J, Wang J, Wu Y, et al. FcγRIIB potentiates differentiation of myeloid-derived suppressor cells to mediate tumor immunoescape. Theranostics. 2022;12(2):842–858. doi: 10.7150/thno.66575.
7. Zahavi D, Weiner L. Monoclonal antibodies in cancer therapy. Antibodies. 2020;9(3):34. doi: 10.3390/antib9030034.
8. Mata-Molanes JJ, Rebollo-Liceaga J, Martínez-Navarro EM, Manzano RG, Brugarolas A, Juan M, Sureda M. Relevance of fc gamma receptor polymorphisms in cancer therapy with monoclonal antibodies. Front Oncol. 2022;12:926289. doi: 10.3389/fonc.2022.926289.
9. Rugo HS, Im S-A, Cardoso F, Cortes J, Curigliano G, Musolino A, Pegram MD, Bachelot T, Wright GS, Saura C, et al. Margetuximab versus trastuzumab in patients with Previously treated HER2-positive advanced breast cancer (SOPHIA): final overall survival results from a randomized phase 3 trial. J Clin Oncol. 2022;41(2):198–205. doi: 10.1200/JCO.21.02937.
10. Vitolo U, Trněný M, Belada D, Burke JM, Carella AM, Chua N, Abrisqueta P, Demeter J, Flinn I, Hong X, et al. Obinutuzumab or rituximab plus cyclophosphamide, doxorubicin, vincristine, and prednisone in Previously untreated diffuse large B-Cell lymphoma. J Clin Oncol. 2017;35(31):3529–3537. doi: 10.1200/JCO.2017.73.3402.
11. Paul S, Konig MF, Pardoll DM, Bettegowda C, Papadopoulos N, Wright KM, Gabelli SB, Ho M, van Elsas A, Zhou S, et al. Cancer therapy with antibodies. Nat Rev Cancer. 2024;24(6):399–426. doi: 10.1038/s41568-024-00690-x.
12. Ravetch JV, Kinet JP. Fc Receptors. Annu Rev Immunol. 1991;9(1):457–492. doi: 10.1146/annurev.iy.09.040191.002325.
13. Sutton BJ, Davies AM, Bax HJ, Karagiannis SN. IgE antibodies: from structure to function and clinical translation. Antibodies. 2019;8(1):19. doi: 10.3390/antib8010019.
14. Gould HJ, Sutton BJ, Beavil AJ, Beavil RL, McCloskey N, Coker HA, Fear D, Smurthwaite L. The biology of IgE and the basis of allergic disease. Annu Rev Immunol. 2003;21(1):579–628. doi: 10.1146/annurev.immunol.21.120601.141103.
15. Pellizzari G, Hoskin C, Crescioli S, Mele S, Gotovina J, Chiaruttini G, Bianchini R, Ilieva K, Bax HJ, Papa S, et al. IgE re-programs alternatively-activated human macrophages towards pro-inflammatory anti-tumoural states. EBioMedicine. 2019;43:67. doi: 10.1016/j.ebiom.2019.03.080.
16. Chauhan J, McCraw A, Nakamura M, Osborn G, Sow H, Cox V, Stavraka C, Josephs D, Spicer J, Karagiannis S, et al. IgE antibodies against cancer: efficacy and safety. Antibodies. 2020;9(4):e55. doi: 10.3390/antib9040055.
17. Nakamura M, Souri EA, Osborn G, Laddach R, Chauhan J, Stavraka C, Lombardi S, Black A, Khiabany A, Khair DO, et al. IgE activates monocytes from cancer patients to acquire a pro-inflammatory phenotype. Cancers 2020. 2020;12(11):3376. doi: 10.3390/cancers12113376.
18. Josephs DH, Bax HJ, Dodev T, Georgouli M, Nakamura M, Pellizzari G, Saul L, Karagiannis P, Cheung A, Herraiz C, et al. Anti-folate receptor-α IgE but not IgG recruits macrophages to attack tumors via TNFα/MCP-1 signaling. Cancer Res. 2017;77(5):1127. doi: 10.1158/0008-5472.CAN-16-1829.
19. Chauhan J, Grandits M, Palhares LCGF, Mele S, Nakamura M, López-Abente J, Crescioli S, Laddach R, Romero-Clavijo P, Cheung A, et al. Anti-cancer pro-inflammatory effects of an IgE antibody targeting the melanoma-associated antigen chondroitin sulfate proteoglycan 4. Nat Commun. 2023;14(14):1–18. doi: 10.1038/s41467-023-37811-3.
20. Grandits M, Palhares LCGF, Osborn G, Chauhan J, Stoker K, Sow HS, Adams R, McCraw AJ, Chenoweth A, Vlasova S, et al. Fc-mediated immune stimulating, pro-inflammatory and antitumor effects of anti-HER2 IgE against HER2-expressing and trastuzumab-resistant tumors. J For Immunother Cancer. 2025;13(3):e010945. doi: 10.1136/jitc-2024-010945.
21. Palhares LCGF, Grandits M, Stoker K, Chauhan J, Sow HS, Fruhwirth GO, Tsoka S, Birtley J, Partington L, Wilson T, et al. An IgE antibody targeting HER2 identified by clonal selection restricts breast cancer growth via immune-stimulating activities. J Exp & Clin Cancer Res. 2025;44(1):49. doi: 10.1186/s13046-025-03319-5.
22. Ilieva KM, Fazekas-Singer J, Bax HJ, Crescioli S, Montero-Morales L, Mele S, Sow HS, Stavraka C, Josephs DH, Spicer JF, et al. AllergoOncology: expression platform development and functional profiling of an anti-HER2 IgE antibody. Allergy: Eur J Allergy Clin Immunol. 2019;74(10):1985–1989. doi: 10.1111/all.13818.

23. Spicer J, Basu B, Montes A, Banerji U, Kristeleit R, Miller R, Veal GJ, Corrigan CJ, Till SJ, Figini M, et al. Safety and anti-tumour activity of the IgE antibody MOv18 in patients with advanced solid tumours expressing folate receptor-alpha: a phase I trial. Nat Commun. 2023;14(1):1–11. doi: 10.1038/s41467-023-39679-9.
24. Frangione B, Milstein C, Pink JRL. Immunoglobulins: structural studies of immunoglobulin G. Nature. 1969;221(5176):145–148. doi: 10.1038/221145a0.
25. Lai P-K, Ghag G, Yu Y, Juan V, Fayadat-Dilman L, Trout BL. Differences in human IgG1 and IgG4 S228P monoclonal antibodies viscosity and self-interactions: experimental assessment and computational predictions of domain interactions. Mabs-Austin. 2021;13(1):1991256. doi: 10.1080/19420862.2021.1991256.
26. Lawrence MG, Woodfolk JA, Schuyler AJ, Stillman LC, Chapman MD, Platts-Mills TAE. Half-life of IgE in serum and skin: consequences for anti-IgE therapy in patients with allergic disease. J Allergy Clin Immunol Pract. 2017;139(2):422–428.e4. doi: 10.1016/j.jaci.2016.04.056.
27. Tanner M, Kapanen AI, Junttila T, Raheem O, Grenman S, Elo J, Elenius K, Isola J. Characterization of a novel cell line established from a patient with Herceptin-resistant breast cancer. Mol Cancer Ther. 2005;3(12):1585–1592. doi: 10.1158/1535-7163.1585.3.12.
28. Jia H, Yang H, Xiong H, Luo KQ. NK cell exhaustion in the tumor microenvironment. Front Immunol. 2023;14. doi: 10.3389/fimmu.2023.1303605.
29. Hirata E, Sahai E. Tumor microenvironment and differential responses to therapy. Cold Spring Harb Perspect Med. 2017;7(7):a026781. doi: 10.1101/cshperspect.a026781.
30. Jiang Y, Li Y, Zhu B. T-cell exhaustion in the tumor microenvironment. Cell Death Dis. 2015;6(6):e1792–e1792. doi: 10.1038/cddis.2015.162.
31. Dang X, Guelen L, Lutje Hulsik D, Ermakov G, Hsieh EJ, Kreijtz J, Stammen-Vogelzangs J, Lodewijks I, Bertens A, Bramer A, et al. Epitope mapping of monoclonal antibodies: a comprehensive comparison of different technologies. Mabs-austin. 2023;15(1):2285285. doi: 10.1080/19420862.2023.2285285.
32. Ott PA, Hodi FS, Kaufman HL, Wigginton JM, Wolchok JD. Combination immunotherapy: a road map. J For Immunother Of Cancer. 2017;5(1):16. doi: 10.1186/s40425-017-0218-5.
33. Garrison LP, Babigumira J, Tournier C, Goertz H-P, Lubinga SJ, Perez EA. Cost-effectiveness analysis of pertuzumab with trastuzumab and chemotherapy compared to trastuzumab and chemotherapy in the adjuvant treatment of HER2-positive breast cancer in the United States. Value Health. 2019;22(4):408–415. doi: 10.1016/j.jval.2018.11.014.
34. Courtney PT, Yip AT, Cherry DR, Salans MA, Kumar A, Murphy JD. Cost-effectiveness of nivolumab-ipilimumab combination therapy for the treatment of advanced non–small cell lung cancer. JAMA Netw Open. 2021;4(5):e218787–e218787. doi: 10.1001/jamanetworkopen.2021.8787.
35. Schoch A, Kettenberger, H., Mundigl, O. Charge-mediated influence of the antibody variable domain on FcRn-dependent pharmacokinetics. Proceedings of the National Academy of Sciences; Vol. 112. 2015. p. 5997–6002.
36. Lohse S, Meyer S, Meulenbroek LAPM, Jansen JHM, Nederend M, Kretschmer A, Klausz K, Möginger U, Derer S, Rösner T, et al. An anti-EGFR IgA that displays improved pharmacokinetics and myeloid effector cell engagement in vivo. Cancer Res. 2016;76(2):403–417. doi: 10.1158/0008-5472.CAN-15-1232.
37. Stip MC, Evers M, Nederend M, Chan C, Reiding KR, Damen MJ, Heck AJR, Koustoulidou S, Ramakers R, Krijger GC, et al. IgA antibody immunotherapy targeting GD2 is effective in preclinical neuroblastoma models. J For Immunother Of Cancer. 2023;11(7):e006948. doi: 10.1136/jitc-2023-006948.
38. Zhang C, Sui Y, Liu S, Yang M. In vitro and in vivo experimental models for cancer immunotherapy study. Curr Res Biotechnol. 2024;7:100210. doi: 10.1016/j.crbiot.2024.100210.
39. Gutierrez-Barbosa H, Medina-Moreno S, Perdomo-Celis F, Davis H, Coronel-Ruiz C, Zapata JC, Chua JV. A comparison of lymphoid and myeloid cells derived from human hematopoietic stem cells xenografted into NOD-Derived mouse strains. Microorganisms. 2023;11(6):1548. doi: 10.3390/microorganisms11061548.
40. Ito R, Takahashi T, Katano I, Kawai K, Kamisako T, Ogura T, Ida-Tanaka M, Suemizu H, Nunomura S, Ra C, et al. Establishment of a human allergy Model using human IL-3/GM-CSF–transgenic NOG mice. J Immunol. 2013;191(6):2890–2899. doi: 10.4049/jimmunol.1203543.
41. Guo X, Sun M, Yang P, Meng X, Liu R. Role of mast cells activation in the tumor immune microenvironment and immunotherapy of cancers. Eur J Pharmacol. 2023;960:176103. doi: 10.1016/j.ejphar.2023.176103.
42. Chuang HJ, Chen Y-Y, Chung Y-D, Huang E, Huang CY, Lung J, Chen C-Y, Liao H-F. The immunosuppressive receptor CD32b regulation of macrophage polarization and its implications in tumor progression. Int J Mol Sci. 2024;25(17):9737. doi: 10.3390/ijms25179737.
43. Osborn G, López-Abente J, Adams R, Laddach R, Grandits M, Bax HJ, Chauhan J, Pellizzari G, Nakamura M, Stavraka C, et al. Hyperinflammatory repolarisation of ovarian cancer patient macrophages by anti-tumour IgE antibody, MOv18, restricts an immunosuppressive macrophage: treg cell interaction. Nat Commun. 2025;16(1):2903. doi: 10.1038/s41467-025-57870-y.
44. Bracher M, Gould HJ, Sutton BJ, Dombrowicz D, Karagiannis SN. Three-colour flow cytometric method to measure antibody-dependent tumour cell killing by cytotoxicity and phagocytosis. J Immunological Methods. 2007;323(2):160–171. doi: 10.1016/j.jim.2007.04.009.
45. Bax HJ, Chauhan J, Stavraka C, Khiabany A, Nakamura M, Pellizzari G, Ilieva KM, Lombardi S, Gould HJ, Corrigan CJ, et al. Basophils from cancer patients respond to immune stimuli and predict clinical outcome. Cells. 2020;9(7):1631. doi: 10.3390/cells9071631.